Turbulent Transport on the Endwall in the Region Between Adjacent Turbine Blades

R. J. Goldstein

R. A. Spores

University of Minnesota,
Department of Mechanical Engineering,
Minneapolis, MN 55455

The complex three-dimensional flow in the endwall region near the base of a turbine blade has an important impact on the local heat transfer. The initial horseshoe vortex, the passage vortex, and resulting corner vortices cause large variations in heat transfer over the entire endwall region. Due to these large surface gradients in heat transfer, conventional measurement techniques generally do not provide an accurate determination of the local heat transfer coefficients. In the present study, the heat/mass transfer analogy is used to examine the local transport coefficients for two different endwall boundary layer thicknesses and two free-stream Reynolds numbers. A linear turbine blade cascade is used in conjunction with a removable endwall plate. Naphthalene ($C_{10}H_8$) is cast into a mold on the plate and the rate of naphthalene sublimation is determined at 6000+ locations on the simulated endwall by employing a computer-aided data acquisition system. This technique allows one to obtain detailed contour plots of the local convection coefficient over the entire endwall. By examining the mass transfer contours, it is possible to infer information on the three-dimensional flow in the passage between the blades. Extremely high transport coefficients on the endwall indicate locations of potential overheating and failure in an actual turbine.

Introduction

To increase the efficiency and power of modern aircraft gas turbine engines, designers are continually trying to raise the maximum turbine inlet temperature. Over the last decade the temperature has risen from 1500 K to 1750 K in some high-performance engines. Of this 250 K increase, only about 25 percent can be attributed to improved alloys (Hennecke, 1982). New materials, such as ceramics, could help increase this maximum temperature even more in the future. However, most of the recent improvements in inlet temperature come from better cooling of the blades and a greater understanding of the heat transfer and three-dimensional temperature distribution in the turbine passage. Higher gas temperature generally causes increased blade temperatures and greater temperature gradients, both of which can have a detrimental effect on service life. In some situations, an increase in metal temperature of 15°C can reduce a component's life by half (Metzger and Mayle, 1983).

The goal of gas turbine heat transfer analysis is to obtain a detailed cooling scheme, for the turbines, blades, and endwall structures between the blades, that allows for maximum inlet temperature. Most studies on heat transfer to gas turbine components deal with the two-dimensional flow region far from the blade endwall. Even here, the flow and transport mechanisms are complex. The present study considers the even more complex endwall region and how the endwall secondary flows influence the heat transfer. Analysis of the flow and heat transfer in this region is extremely difficult. Although impressive strides have been made recently in predicting the major secondary flow phenomena (saddle point on endwall, leading edge horseshoe vortex, Hah, 1984), modern computational schemes still do not have the needed accuracy to calculate heat transfer in the endwall region. This implies that at present industry must resort to experimentation for

heat transfer design improvements and the data base needed for future numerical work.

The flow field near the endwall generates a complex pattern in the convective heat transfer distribution on both the passage endwall and the blades. Knowledge of the local heat transfer distribution throughout the passage is essential in understanding the flow field's effect on heat transfer. This study provides detailed results for the endwall region of a particular blade configuration by employing the heat/mass transfer analogy.

Several investigators have already looked at endwall heat transfer in a cascade. Blair (1974) investigated the film cooling effectiveness and convection heat transfer coefficient distributions on the endwall of a large-scale turbine vane passage. Graziani et al. (1980) looked at heat transfer to both the airfoil and the passage endwall in a blade cascade using a series of strip heaters in combination with an array of thermocouples. Georgiou et al. (1979) studied iso-heat-transfer-rate lines on the endwall by using an isentropic compression tube facility along with thin film heat transfer gages. York et al. (1984) obtained endwall heat transfer results using measurements from a double layer grid of thermocouples as input to a finite element solution. A comparison was made by Gaugler and Russell (1984) between heat transfer distributions and visualized secondary flows on a turbine endwall.

The present study uses a mass transfer system to study the transport coefficient on the endwall. Related mass transfer results include: Goldstein and Karni (1984) and Sparrow et al. (1984) who both investigated the effects of an endwall boundary layer on a cylinder in crossflow using mass transfer; Goldstein and Taylor (1982) looked at mass transfer in the neighborhood of film cooling holes. In addition, Kan et al. (1971) conducted a local mass transfer experiment on a two-dimensional blade in a cascade.

One important advantage of the mass transfer technique is that much greater detail of the local transfer coefficient can be obtained. In the present study, measurements were taken at

6387 locations over the test area, in comparison to fewer than 200 points for any of the previous endwall studies. Another advantage of mass transfer is that regions of high gradients are more easily determined; conduction in the test plate that smooths out local extremes in heat flux is not a problem.

Experimental Apparatus and Procedure

This study has been carried out at the University of Minnesota Heat Transfer Laboratory using an open circuit wind tunnel with a test section 46.9 cm wide by 60 cm high. The test section has a steel floor, plexiglass sides and top, and contains a rectilinear turbine blade cascade consisting of six scaled-up high-performance (G.E. CF6-50 Stage One High Pressure) turbine blades running the height of the test section. The blades have a chord length and aspect ratio of 16.91 and 3.55, respectively. The turbine blade coordinates can be found in Ito (1976). The top of the test section has a hole cut out for the insertion of a test plate, which contains a flat molded-naphthalene surface positioned on top of the third, fourth, and fifth blades of the cascade.

A drawing of the test plate used to contain the naphthalene is shown in Fig. 1. The leading edge of the plate is at the same angle to the oncoming flow as the cascade to provide similar upstream boundary conditions for equivalent locations in both of the active mass transfer endwall passages. Three thermocouples are embedded just under the naphthalene surface at different positions on the plate. These thermocouples measure the temperature near the naphthalene–air interface to determine the surface vapor pressure. All thermocouple readings are within 1 mV (~ 0.02°C) of each other, indicating that the temperature variation along the plate is insignificant.

A brief outline of the data acquisition system follows; a more complete discussion of the system is given by Goldstein et al. (1985). Two stepper-motor-driven positioning tables provide controlled measurement over the entire naphthalene surface. The test plate is mounted on the lower positioning table while the upper table moves a depth gage over the naphthalene surface. This depth gage is a Linear Variable Differential Transformer (LVDT) with a linear operating range of 0.020 in. (0.51 mm) and resolution of about 2.0 μin. (50 μm). The LVDT is connected to a signal conditioner, which supplies excitation and converts the a-c signal output of the gage to a calibrated d-c voltage. A voltmeter reads the voltage output and sends the signal to a minicomputer for data reduction. To control the stepper-motors, a HP-85 microcomputer is used. Between this computer and the motors is a hardware interfacing component, which converts the HP-85 commands from digital signals into a number of properly se-
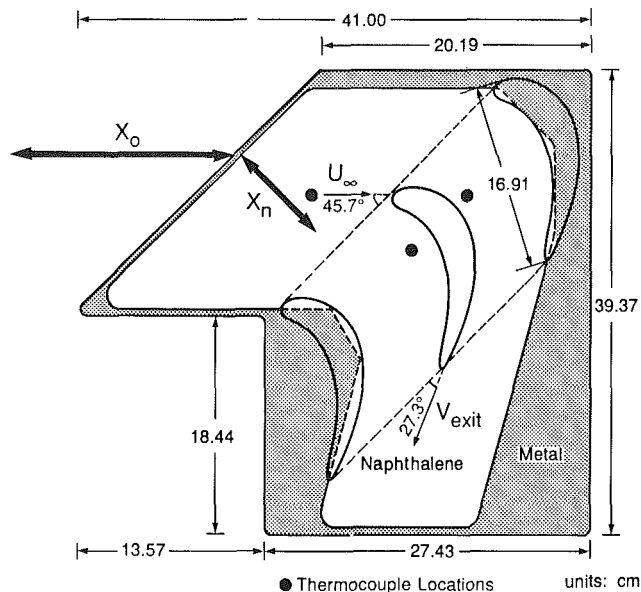

Fig. 1 Test plate showing naphthalene surface

quenced phase control signals, which instruct the stepper-motors physically to move.

Prior to a wind tunnel test, the test plate, which has been cast with naphthalene, is mounted on the lower positioning table of the data acquisition system. The initial naphthalene surface profile is measured over a specified nonuniform rectangular grid of points on the test plate. In regions where steep gradients are known to exist (from preliminary tests), more points are taken. After these initial measurements, the plate is removed from the positioning tables, enclosed in a special carrying case (to eliminate sublimation during transport), and moved to the wind tunnel room. The test plate is placed in the test section on top of the turbine blades and exposed to the air stream for a period of 90–120 min, depending on run conditions. A second set of naphthalene surface measurements is taken next at the same specified locations on the test plate as the preliminary measurements. Reference points on the metal surface are also taken during the initial and final runs. These reference points are used to calculate reference planes from which the local naphthalene surface profiles are measured. The actual amount sublimed at each location is determined by subtracting the final local measurement from the initial one, where both measurements are taken with respect to their reference planes. Based on test conditions and the amount of

Nomenclature

C = axial chord length = 16.91 cm
D = diffusion coefficient
h_m = local mass transfer coefficient
h_{mo} = local mass transfer coefficient for flat plate case
Pr = Prandtl number = ν/α
Re_c = free-stream Reynolds number based on axial chord length and U_∞
Re_x = Reynolds number based on distance from virtual origin to location of interest and U_∞
Sc = Schmidt number = ν/D

St_h = local heat transfer Stanton number
St_{ho} = local heat transfer Stanton number for flat plate case
St_m = local mass transfer Stanton number = h_m/U_∞
St_{mo} = local mass transfer Stanton number for flat plate case = h_{mo}/U_∞
T = local temperature
U = local flow velocity
U_∞ = mean velocity of approaching main stream flow, measured 22.9 cm upstream of blade leading edge
U_{exit} = mean velocity of flow leaving turbine passage

w = mass concentration
X = effective distance from the virtual origin of the turbulent boundary layer to location of interest in a turbine passage = $X_n + X_o$
X_n = the portion of length X actually on the naphthalene surface
X_o = distance from virtual origin of boundary layer to the start of the naphthalene surface
y = distance from endwall
α = thermal diffusivity
δ = boundary layer thickness
ν = kinematic viscosity

naphthalene sublimed, the local mass transfer Stanton number is calculated. Note that sublimation occurs continuously throughout the measurement process, but even at the locations of least mass transfer this is only about 7 percent of the total local sublimation. A correction is applied in the data reduction for the amount sublimed during handling and the measurement process. For all data runs, the maximum sublimation never exceeded 0.254 mm (0.01 in.) or 0.15 percent of the blade's chord length; thus change in geometry of the passage is not a problem.

An uncertainty analysis using the method outlined in Moffat (1982) reveals that the technique used has an overall error margin of 4.7 percent. The largest sources of uncertainty are in the test plate alignment process and in the naphthalene vapor pressure, which is used to calculate the mass transfer Stanton numbers. Deviations between the individual runs are usually less than 3 percent in the passage, while slightly greater discrepancies were found in the region upstream of the blades. Preliminary tests that included several passages showed that the periodicity of the measurements from blade passage to passage are likewise typically within 3 percent.

Heat–Mass Transfer Analogy

The analogy is based on the fact that the governing differential equations for mass and energy transport are essentially the same. One merely has to replace the nondimensional parameters in the energy equation by the corresponding parameters (e.g., T and Pr, by w and Sc) to obtain the mass transfer equation. This analogy is valid only for a constant property fluid, which can be assumed as long as the transported quantities (heat or mass) are not creating large gradients in the flow (Eckert, 1972, 1976). In using mass transfer results for heat transfer predictions, care must be taken when the value of the Schmidt number in the mass transfer study differs from the Prandtl number in the heat transfer application. Basically this is equivalent to doing a parallel heat transfer study with a fluid of different Prandtl number from the one of interest in an application. In either event, one needs to be aware that there is a variation in convective transport with Prandtl (Schmidt) number and that this variation is generally a function of both geometry and Reynolds number. Many analogies and anslyses have been used to predict this Prandtl number variation in pure heat transfer cases, but even today this is not completely established, especially with intense vortices such as those encountered in the present work. Although the Schmidt number for naphthalene diffusion in air is approximately 2.0,[1] the primary application for turbine heat transfer would be in air, which has a Prandtl number of approximately 0.7. This difference (2.0 versus 0.7) is relatively small compared to variations that occur in a number of other mass/heat transfer analogies. Even so, it is desirable to reduce the problem of comparing heat (or mass) transfer results using several fluids, each with a different Prandtl (or Schmidt) number, by using relative measurements. In the present study this means dividing the local mass transfer results in a turbine passage (St_m) by the local mass transfer measurements taken on the flat surface in the absence of turbine blades (St_{mo}) to give a ratio, St_m/St_{mo}. There still could be a Prandtl (Schmidt) number influence when translating this to a different Prandtl (Schmidt) number since the Stanton number variation with Prandtl (Schmidt) number could be different for the cases with and without blades present. However, it appears to be a

[1]The value of Sc chosen does not significantly affect St_m/St_{mo} in the present study because of the small range of test conditions. This value is somewhat different from that usually used in the past, which comes from a re-analysis of data for the diffusion coefficient. A review of the mass transfer physical properties is being prepared for publication.
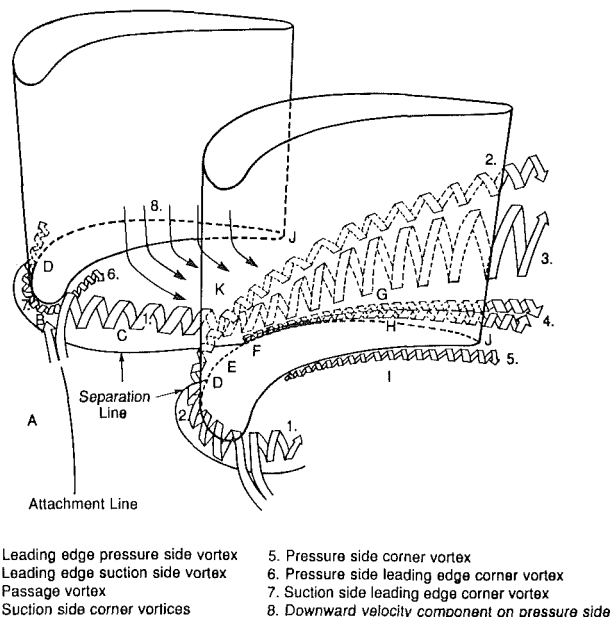

Fig. 2 The three-dimensional flow field in the endwall region

1. Leading edge pressure side vortex
2. Leading edge suction side vortex
3. Passage vortex
4. Suction side corner vortices
5. Pressure side corner vortex
6. Pressure side leading edge corner vortex
7. Suction side leading edge corner vortex
8. Downward velocity component on pressure side

reasonable approach because the difference in Prandtl (Schmidt) number dependence for the two cases is probably not very large.

The values of St_{mo}, actually used, are determined experimentally in the same test section and under the same conditions as St_m with the exception that the blades are absent. For verification, the values of St_{mo} are also compared with a standard correlation and found to be in good agreement. Flat plate mass transfer Stanton numbers can be calculated using a relation by von Karman between the coefficients of heat transfer and skin friction along with an equation for local skin friction along a flat plate (Schlichting, 1979). An expression for the unheated starting length is added and then the heat–mass transfer analogy is employed. The final equation used is

$$St_{mo} = \frac{1.60 \, (\ln Re_X)^{-2.584}}{1 + 14.62 \, (\ln Re_X)^{-1.292}} \left[1 - \left(\frac{X_0}{X} \right)^{.9} \right]^{-1/9}$$

A 3 percent difference between experiment and calculations is observed for the main test case. When calculating St_{mo} for each particular point in a run, a length X is used from the effective origin of the turbulent boundary layer. The question then arises as to how this length should be taken on the naphthalene surface between the blades. It was decided to take that portion of length X that lies on the plate surface, X_n, as the perpendicular distance from the leading edge of the naphthalene to the particular point of interest, instead of a curved streamline through the passage (see Fig. 1).

Flow Field

The heat (mass) transfer variation in the endwall region is closely related to the fluid flow in the turbine passage. For this reason, a discussion of the fluid mechanics inside a turbine passage is a prerequisite to discussing the results. Figure 2 shows our present concept of the fluid mechanics in the passage. Much of this is derived from flow visualization and direct measurements by a number of investigators including: Marchal and Sieverding (1977), Langston (1980), Sieverding (1985), and Sonoda (1985). Figure 2 shows the major vortices, labeled 1 through 7, and the primary regions of interest, labeled A through K, in the passage. The secondary flows of the endwall region are primarily the result of two main pressure gradients in the passage. The pressure variation at the leading edge–endwall intersection (due to both the boundary

layer velocity distribution and the stagnation of flow on the blade) forces the flow down toward the endwall, where it rolls up into the leading edge (horseshoe) vortex. The two legs of the leading edge vortex can be seen in Fig. 2 as Vortices 1 and 2. The turning of the mainstream flow between the turbine blades results in the second pressure variation – a strong gradient across the passage. This gradient affects the paths of both legs of the leading edge vortex and the low-momentum flow adjacent to the endwall. It also generates a downflow on the pressure surface and upflow on the convex surface. The concave (pressure) side leg of the leading edge vortex (Vortex 1) combines with the low-momentum flow near the endwall to form what is known collectively as the passage vortex (Vortex 3). Upon reaching the suction side, the passage vortex lifts off the endwall and continues downstream along the suction side of the passage. In contrast, the suction side leg of the leading edge vortex (Vortex 2) continues from its inception, along the blade–endwall junction until it reaches the separation line of the endwall boundary layer at region D. At the separation line the suction side leg of the leading edge vortex lifts off the endwall and continues downstream along the suction surface adjacent to the passage vortex. Sieverding (1985) indicates that Vortex 2 wraps itself around the passage vortex and the actual position of Vortex 2 depends on cascade geometry and overall flow conditions. Both Vortices 1 and 2 are believed to lift off the endwall surface due to the higher average velocities, and lower pressures, found away from the endwall along the suction surface.

Two reference lines are shown in the endwall flow visualization photograph, Fig. 3 (Goldstein and Chen, 1985). S_1–S_2 delineates the separation line of the endwall boundary layer as it approaches the turbine blades. A_1–A_2, often called the attachment line, extends from the incoming flow to the stagnation point on the front of the turbine blade. This attachment line divides the incoming boundary layer flow entering a blade passage from the flow entering the adjacent passage. The intersection of these two lines is a saddle point.

The transverse pressure gradient affects the mainflow as much as a chord length away from the endwall. For example, the downwash (toward the endwall) on the pressure surface is so strong that flow visualization by Marchal and Sieverding (1977) reveals a small corner separation line in the endwall region of the pressure side. They likewise observed a suction side–endwall corner separation similar to the one on the pressure side and believe that both separation lines are accompanied by small vortices (Vortices 4 and 5); further justification of Vortices 4 and 5 will be shown in the present study. Note that near the suction side corner, both the mass transfer results of the present study and the work of Sonoda (1985) imply the existence of two suction side corner vortices. These suction side corner vortices originate just downstream of where the passage vortices lift off from the endwall (region F) and appear to be driven by an interaction of the passage vortex with the suction surface. The pressure side corner vortex first becomes apparent on the endwall approximately 1/3 of the way back from the blade's leading to its trailing edge.

Sonoda (1985) discusses in more detail the development of the suction side corner vortex pair. He found these vortices originate just downstream of the S_1–S_2 separation line near the suction surface and are slightly away from the endwall, whereas this study observes the effects of this pair directly on the endwall. Sonoda suggests that these vortices form due to an interaction of the leading edge suction side vortex (instead of passage vortex as suggested above) with the suction surface.

The formation of the leading edge (horseshoe) vortex acts as the driving force for another corner vortex. The leading edge corner vortices (referring to Vortices 6 and 7), which are the most intense vortices in a turbine blade passage, originate in the same region as the horseshoe vortex but have a rotation in the opposite direction. This observation of an intense corner

Fig. 3 Flow visualization of endwall (Goldstein and Chen, 1985)

Table 1 Test conditions

	Case 1	Case 2	Case 3
Free-stream velocity	13.19 m/s	13.23 m/s	8.23
Reynolds number Re_c	1.42×10^5	1.42×10^5	8.86×10^4
Boundary layer thickness 0.99U	1.504 cm	2.913 cm	1.171 cm
Displacement thickness	0.213 cm	0.378 cm	0.170 cm
Momentum thickness	0.151 cm	0.284 cm	0.116 cm
$U/U_\infty = (y/\delta)^{1/n}$	$n = 5.90$	$n = 6.90$	$n = 5.43$
Turbulence intensity	1.20%	1.20%	1.22%
St_{mq} (at leading edge of blades)	1.472×10^5	1.376×10^{-3}	1.563×10^{-3}

vortex underneath the horseshoe vortex is also found at the front base of a circular cylinder in crossflow (Goldstein and Karni, 1984).

The final region to be discussed is the wake region just downstream of the turbine blade trailing edge (region J). As the high-pressure fluid from one side of the blade meets the low-pressure fluid from the other side, a highly mixed and large eddy flow region results. Gaugler and Russell (1984) observed a diverging flow pattern on the endwall in this region by using ink dot flow visualization. This seems to indicate an impingement of flow onto the endwall, which as seen later results in high local heat transfer coefficients.

Operating Conditions

Three test conditions were studied, encompassing two Reynolds numbers and two separate boundary layer thicknesses. The mainstream velocities used are 8.2 m/s and 13.2 m/s. In the mainstream flow, the turbulence intensity is measured via hot-wire anemometry as 1.22 percent for the low-speed case and 1.20 percent for the higher speed. The turbulence measurements were taken in the free stream 21 cm in front of the cascade and in the middle of the test section. Test conditions for the three cases studied are summarized in Table 1.

The free-stream velocity is measured at a point 22.9 cm in front of the cascade, while all boundary layer measurements are taken 15.2 cm in front of the cascade.

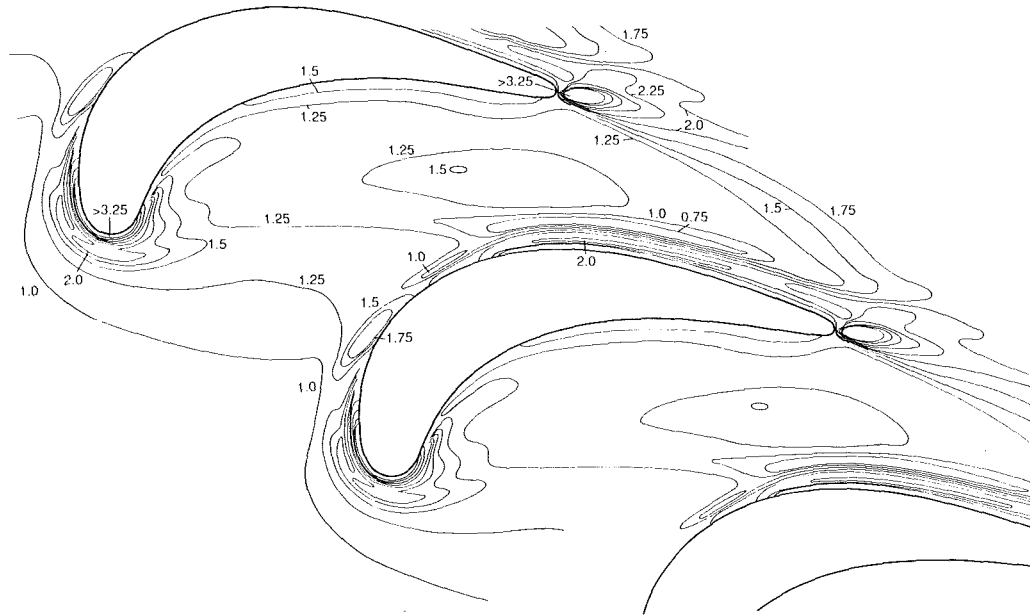Temperature variation throughout the run is kept to within 0.20°C, which corresponds to a 2.0 percent variation in

Fig. 4(a)   Case 1, main test case; contours of St_m/St_{mo} = 0.75, 1.0, 1.25, 1.5, 1.75, 2.0, 2.25, 2.5, 2.75, 3.0, 3.25
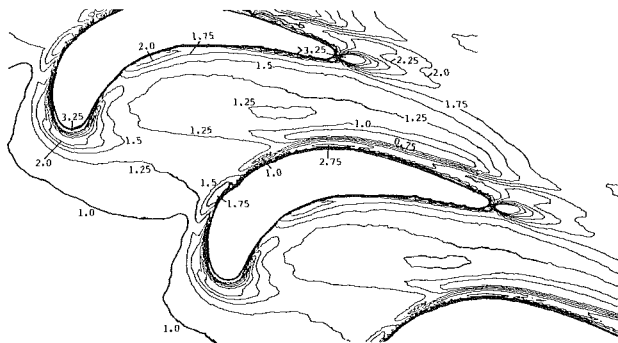

Fig. 4(b) Case 2, thick boundary layer case; contours of St_m/St_{mo} = 0.75, 1.0, 1.25, 1.5, 1.75, 2.0, 2.25, 2.5, 2.75, 3.0, 3.25
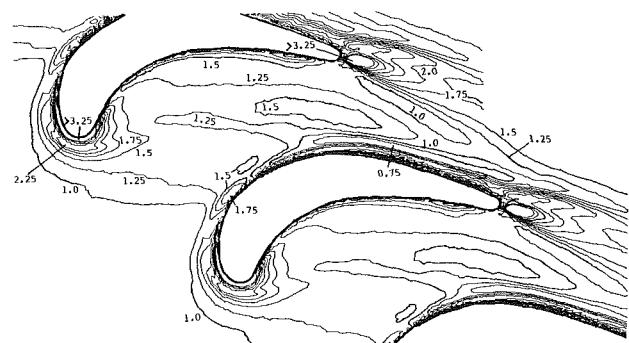

Fig. 4(c)   Case 3, low Reynolds number case; contours of St_m/St_{mo} = 0.75, 1.0, 1.25, 1.5, 1.75, 2.0, 2.25, 2.5, 2.75, 3.0, 3.25

naphthalene vapor pressure. The vapor pressure of naphthalene, and consequently the sublimation rate, are highly dependent on surface temperature. Accurately monitoring and stabilizing the temperature is critical in naphthalene mass transfer experiments.

The constant vapor pressure condition that exists over the naphthalene endwall corresponds to an isothermal boundary condition for the heat transfer case, while the non-naphthalene turbine blades correspond to adiabatic walls in heat transfer. These boundary conditions differ from those in an actual turbine passage where the blades and endwall are all active. This is not considered a significant problem. Other mass transfer studies with simpler geometries have shown only minor differences between having active or inactive boundaries adjacent to the surface of interest.

Results – Mass Transfer on the Endwall

Nondimensionalized mass transfer contours of constant St_m/St_{mo} for Case 1 (the main test case) are shown in Fig. 4(a). Figures 4(b) and 4(c) represent runs with a thickened boundary layer (Case 2) and a lower Re_c (Case 3), respectively. These figures are generated using a computer plotting program that interpolates between the data points to draw line segments. Note that smoothing out of the contour lines is involved and that these figures, which show mass transfer for two adjacent passages, are actually the data from just one rectangular region, printed twice. The steep reduction in mass transfer

near the turbine blades results in many contour lines around the blade surfaces; note that the mass transfer actually goes to zero right at the turbine surfaces. These lines adjacent to the blades have been eliminated for clarity. Figure 4(a) is a completely smoothed-out version while Figs. 4(b) and 4(c) show the original computer-generated contours. Case 1 will be discussed in detail with follow-up comments on how the other cases deviate from Case 1. The regions referred to in the discussion are shown on Fig. 2.

Mass transfer for the endwall region upstream of the turbine cascade (region A) is essentially that for an isothermal flat plate and the ratio equals just under 1.00. As the flow approaches the leading edge of a turbine blade (region B), a sharp increase in mass transfer is noticed as a result of the rollup of the oncoming boundary layer into the horseshoe vortex, which scrubs this area of the endwall very effectively. The Stanton number ratio increases up to its highest value on the endwall, St_m/St_{mo} = 5.28, very close to the leading-edge–endwall junction as a result of the intense leading edge corner vortices, which wrap tightly around the front of the blade. Figure 5 is a one-dimensional plot showing the variation in St_m/St_{mo} straight out (into the direction of U_∞) from the leading edge of a blade. Note the double maximum in the profile; the dominant peak is a result of the leading edge corner vortex while the lesser peak is a result of the horseshoe vortex.

The contour plots show a rapid decrease in mass transfer as both sets of leading edge vortices travel around the blade. The
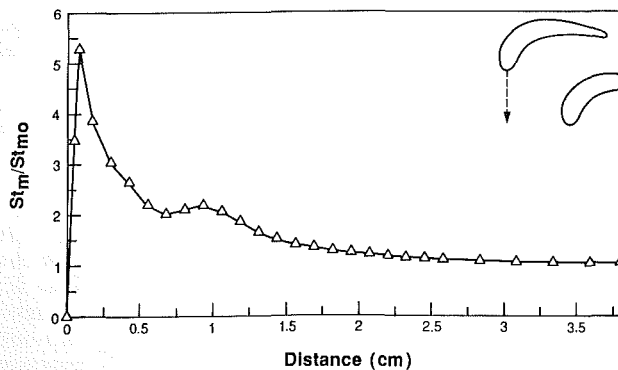
Fig. 5 St_m/St_{mo} versus distance from leading edge (Case 1)

Fig. 6 St_m/St_{mo} versus distance across passage (Case 1)

leading edge suction side vortex quickly lifts off the endwall as it traverses around the nose and the suction leg of the leading edge corner vortex does likewise. As these suction side vortices separate they create a small region of relatively low mass transfer on the endwall where $St_m/St_{mo} \sim 1.0$ (region D). The leading edge region of high mass transfer continues around the concave side as a result of the pressure side leg of the leading edge corner vortex (Vortex 6). As on the suction side, the Stanton number ratio quickly drops off close to the wall as Vortex 6 appears to diminish or lift off the endwall. In contrast, Vortex 1 affects a much larger area, region C.

The passage vortex increases the ratio of St_m/St_{mo} up to 1.36 in a band (region C) extending from the leading edge of one blade to the suction surface of the adjacent blade. Note that in the separation region just upstream of the passage vortex, near where the fluid lifts off the endwall or changes direction by approximately 90 deg in order to flow with the vortex, there is no noticeable reduction in mass transfer. However, near where the passage vortex encounters the suction surface there is a relatively large increase in mass transfer on the upstream side of the location (region E) and low mass transfer on the downstream side (region F).

The high mass transfer zone, region E, is the result of a localized region of highly turbulent flow caused by the transverse pressure gradient turning the upstream boundary layer flow and forcing it to flow toward the suction surface. Note that this local peak (region E) occurs in front of the separation line and is consequently not believed to be the result of a stagnation point due to the passage vortex. The low mass transfer area, region F, on the other hand is due to a "dead zone" on the surface, created underneath the lift off of the passage vortex as it climbs up the suction surface.

The midpassage of the endwall, region K, is an area of approximately uniform mass transfer, which contrasts to large variations near the suction surface and the increase near the pressure side. Figure 6 is a one-dimensional plot of St_m/St_{mo} through region K from pressure side to suction side taken 70 percent of the chord length back from the leading edge. This figure reveals a slight peak in mass transfer near the concave side, due to the weak pressure side corner vortex (region I, Vortex 5) generated under the downwash from the pressure surface. This pressure side corner vortex increases the convection ratio, St_m/St_{mo}, to 1.56. Near the suction side, Fig. 6 shows a dramatic decrease in mass transfer where the boundary layer separates off the endwall (region G), followed by a strong increase as a result of the suction side corner vortices (region H).

The narrow strip of reduced mass transfer, region G, is due to separation of the new passage boundary layer (which forms behind Vortex 1) as it feeds the passage vortex, which at this point is well off the endwall and traveling along the suction surface. This strip is the largest region on the endwall where the flow pattern reduces the mass transfer below the flat plate case. In region G, St_m/St_{mo} decreases to as low as 0.44 (cf.
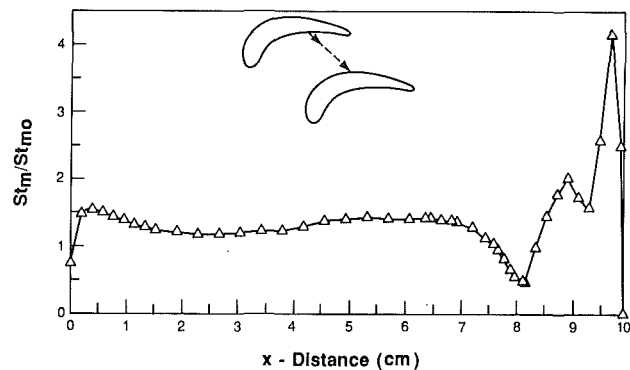
Fig. 6). Note in Fig. 4(a) that the lowest contour shown in this region is 0.75 as the 0.5 contour would be an extremely narrow strip.

Closer to the suction surface (region H), the mass transfer steeply increases again as a result of the two suction side corner vortices (Vortices 4 in Fig. 2). Although only affecting a thin region in the corner, the vortex closest to the suction surface on the endwall attains a peak mass transfer ratio, $St_m/St_{mo} = 4.2$, while the outer vortex of the pair attains a maximum of approximately half this value. Both strips of increased convection start at region F on the endwall but are indistinguishable from one another at the trailing edge where both have a Stanton number ratio of about 2.0. The increased transport caused by the inner (more intense) suction side corner vortex has reduced to $St_m/St_{mo} \sim 3.0$ by the 80 percent axial chord point through the passage.

In addition to the extensive increase in mass transfer at the leading edge and along the suction surface of the blade, another significant increase can be found at the blade trailing edge (region J). A double peak in mass transfer is found in this region with the more significant peak a result of the strong recirculating wake behind the blade. The lesser peak, always located on the suction side of the main peak, is believed to be caused by the suction side corner vortices continuing past the blade trailing edge to interact with the recirculating fluid and form another region of large eddies. The primary peak reaches a St_m/St_{mo} ratio of 4.6 while the lesser peak is 2.25. Figure 7 is a graph of St_m/St_{mo} from the trailing edge of a blade through the primary peak in mass transfer induced by the recirculation fluid. The peak coincides with the direction of the exit velocity in the passage. Note that the Stanton number ratio remains about 2.0 well downstream of the trailing edge.

Effect of Thicker Boundary Layer. The differences between test Cases 1 and 2 (Figs. 4a and 4b) are rather minor. The displacement thickness has been increased by 77 percent for Case 2 by placing a trip wire on the test section floor 50 cm upstream of the cascade. Note that the St_m/St_{mo} contours are very similar for both cases. Both figures show the 0.75 contour just off the suction surface and peaks in excess of 3.25 over similar-sized areas at both the leading and trailing edges of the blades. Further, it appears that the thicker boundary layer has little effect on the mass transfer in region C; the horseshoe vortex causes essentially the same increase in mass transfer for both test cases.

There are, however, some small differences in the mass transfer between Case 1 and Case 2. The contour plots indicate that for Case 1 the mass transfer near the pressure side is larger; it is over 2.0 for the thick boundary layer case while it only reached a maximum of 1.56 for Case 1. Also note how the mass transfer ratio is greater than 1.25 near the pressure surface over a much greater area for Case 2. This increased mass transfer indicates that the downwash off the pressure surface and/or the pressure side corner vortex are stronger for
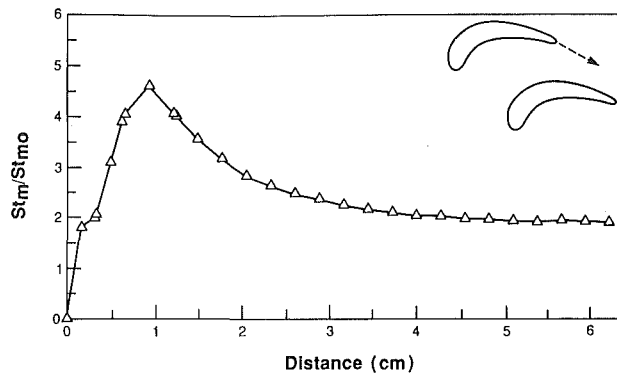
Fig. 7 St_m/St_{mo} versus distance from trailing edge

Fig. 8 Average St_m/St_{mo} along turbine passage

the thick boundary layer case. In contrast, mass transfer in the midpassage and near the suction side is smaller for the thicker boundary layer case. The reduction at midpassage is best seen by comparing the closed contour of $St_m/St_{mo} = 1.25$ at midpassage for both cases. From the St_m/St_{mo} contours of 1.0 and 0.75 in region G it is apparent that the reduction in mass transfer for Case 2 continues all the way to the suction surface. Interestingly, the reduced mass transfer from midpassage to the suction surface nearly compensates for the increase near the pressure surface to yield average values across the passage that are nearly equal for the two flow conditions.

Effect of Changing Reynolds Numbers. Between Cases 1 and 3 there is a decrease in Reynolds number of 38 percent and a decrease in displacement thickness of 20 percent. Even though the differences in mass transfer ratio are again not large, they are more pronounced than between Cases 1 and 2. First, Case 3 indicates an increase in mass transfer over Case 1 in the center of the passage where a larger portion of area is enclosed by both the 1.25 and 1.5 contours. However, the contour plots are somewhat misleading and this increase is not really significant. Although a larger area at midpassage is enclosed by the 1.5 contours for the lower Reynolds number (Case 3), the same area has a St_m/St_{mo} ratio just below 1.5 (at about 1.45) for Case 1. Another difference can be seen at the exit plane of the cascade. Notice the closed contour of $St_m/St_{mo} = 1.0$ just upstream of the gradual rise in mass transfer from the wake behind each turbine blade; this contour is absent in the other test cases. The drop in mass transfer appears to be the result of a stagnant zone that occurs as the endwall boundary layer encounters the wake from the pressure side blade of the passage. It also should be pointed out that Case 3 has a significantly lower average value of St_m/St_{mo} downstream of the blades, which can be attributed to the area of reduced mass transfer (region G) extending well past the trailing edge.

Average Mass Transfer in the Passage. Figure 8 is another approach to presenting the mass transfer data. The Stanton number ratio for a strip of endwall across the passage is averaged and plotted as a function of the distance transversed through the passage. This graph of average St_m/St_{mo} is slightly biased upstream and downstream of the cascade since only the rectangular regions shown in the contour plots are included in the averaging. The ratio is 1.0 upstream of the blades (as expected), but quickly rises near the line connecting the leading edges of the blades. This steep increase is a result of the two leading edge vortices (horseshoe and leading edge corner), which greatly increase the mass transfer. Downstream of this peak there is a sharp minimum in the average mass transfer. This region of reduced mass transfer corresponds to the area just downstream of the passage vortex sweeping across the endwall; in this region the boundary layer is starting over and the momentum of the flow is weak. Another significant finding observed on this graph is that the turbulent wake
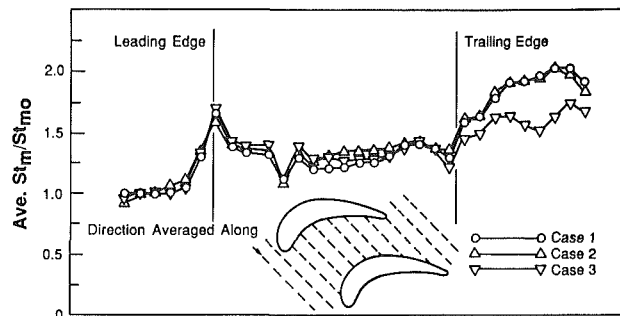
behind the blades results in an average convection coefficient double that for the flat plate case.

Note how the profiles follow one another for all three test cases. As mentioned earlier, the averages for Cases 1 and 2 are nearly the same even though the mass transfer is greater near the pressure surface and less near the suction surface for the thicker boundary layer flow. The only significant deviation among the three cases is in the wake region where the flow in Case 3 (lower Reynolds number) results in a much lower average value as the strip of reduced mass transfer (region G) extends past the trailing edge to cover a much greater area.

The differences among the contour maps themselves are minor. The fact that the results are quite similar despite significant variation in the parameters is not unusual. Georgiou et al. (1979) and Graziani et al. (1980) likewise found little disparity in the contours as the major parameters were changed. Differences between runs are even less for this study because variations in the boundary layer thickness and Reynolds number are taken into account in the divisor St_{mo}. For example, St_{mo} is about 6.5 percent lower over the endwall for the thicker boundary layer case and about 6.2 percent higher for the low Re_c case, both compared to Case 1. However, St_m with the blades present also varies by similar amounts yielding ratios that are approximately equivalent to the main test case.

When the ratio St_m/St_{mo} is averaged over the entire endwall region between adjacent turbine blades, from the leading edges of two blades to the trailing edges (i.e., in the region between the two vertical lines shown in Fig. 8), the overall average Stanton number ratio is found to be 1.31 for Case 1. The secondary flows increase the convection mass transfer on the endwall by 31 percent over the flat plate case.

Comparison With Heat Transfer Results. Comparisons were made of the transport coefficients measured in this study with the results of Blair (1974), Georgiou et al. (1979), Graziani et al. (1980), Gaugler and Russell (1984), and York et al. (1984). It should be pointed out that all these studies, except Graziani et al. (1980), are for inlet guide vanes, unlike the present study, which takes measurements around a rotor blade. Blair (1974) and Georgiou et al. (1979) present results similar to each other with the minor difference that Georgiou et al. (1979) reports two regions of low heat transfer, one near the inlet at midpassage and the other a strip just off the suction surface, farther upstream than Blair does. The data of Gaugler and Russell (1984) and York et al. (1984) show the same trends of reduced heat transfer plus quite distinctly revealing regions of increased heat transfer at both the leading edges of the blades (due to the horseshoe vortices) and in the blade wake region (due to the mixing of pressure and suction side flows). All these major trends are also found in the data presented here; however, the region of reduced (mass) transfer near the inlet of the passage is only subtly shown while the other features are obvious from the contour maps. The region of reduced transfer can best be seen in Fig. 8, which shows a

large decrease in average mass transfer downstream of the leading edge.

The data of Graziani et al. (1980) agree the best with the present study, particularly their thick boundary layer case and the thick boundary layer case of this report. Although the free-stream Reynolds number is four times greater for Graziani, both cases have virtually identical displacement thicknesses. In addition to agreeing with the major trends already pointed out, the two studies also agree in magnitude and area on the effect from the leading edge vortex traversing the endwall between blades. Their thick boundary layer case even shows hints of two vortices at the blade leading edge. A one-dimensional comparison was made between strip-averaged values across the passage for St_m/S_{mo} from this study and strip-averaged values for St_h/St_{ho} from their thick boundary layer case. Except for the region close to the trailing edge, the agreement is within 10 percent throughout the passage.

Contributions to the current understanding of heat transfer on the endwall not found in previous studies include: observing an increase in the convection on both the pressure side–endwall junction and the suction side–endwall junction from corner vortices; although the study of Graziani et al. (1980) shows some signs of the leading edge corner vortex, the present study is the first to reveal the effects of this vortex in detail. The other studies, which used heat transfer, do not show as great extremes in convective coefficient values or as much detail in their contour maps.

Summary and Conclusions

1. Much greater detail of the convection process can be obtained using a local mass transfer technique as compared with conventional heat transfer instrumentation. Regions of high turbulent transport are more easily determined using mass transfer since conduction in a test plate tends to smooth out regions of high heat transfer gradient. Due to the potentially greater density of measurement locations, it is much easier to correlate the convection patterns with the secondary flows than in heat transfer studies. The mass transfer results can be used to predict the heat transfer for an equivalent flow.

2. Presenting the data in the form of St_m/St_{mo} appears to be a convenient way of expressing the results. As shown in Fig. 8 and by an examination of the contour plots, data from all three test cases are very similar when standardized in this manner.

3. This study helps to confirm the existence of several flow features in a turbine cascade that have only recently been observed. These features include the corner vortices at the pressure side–endwall junction, the pair of vortices at the suction side–endwall junction, and the leading edge corner vortices.

4. The secondary flows in a turbine passage result in a complex distribution of convection coefficients that vary by more than an order of magnitude over the endwall. Two-dimensional boundary layer analysis would not accurately describe the variations in convection throughout the passage.

5. The secondary flow between turbine blades has an overall effect of increasing convection on the passage endwall

by a factor of 1.31 over the flat plate case. However, localized increases up to 5.28 are present, which, with the large gradients in transport coefficient, could lead to significant thermal stresses.

References

Blair, M. F., 1974, "An Experimental Study of Heat Transfer and Film Cooling on Large-Scale Turbine Endwalls," ASME JOURNAL OF HEAT TRANSFER, Vol. 96, p. 524.

Eckert, E. R. G., and Drake, R. M., 1972, *Analysis of Heat and Mass Transfer*, McGraw-Hill, New York, p. 728.

Eckert, E. R. G., 1976, "Analogies to Heat Transfer Processes," *Measurements in Heat Transfer*, Hemisphere Publishing, New York, pp. 399–403.

Gaugler, R. E., and Russell, L. M., 1984, "Comparison of Visualized Turbine Endwall Secondary Flows and Measured Heat Transfer Patterns," ASME *Journal of Engineering for Gas Turbines and Power*, Vol. 104, p. 715.

Georgiou, D. P., Godard, M., and Richards, B. E., 1979, "Experimental Study of the Iso-Heat-Transfer-Rate Lines on the End-wall of a Turbine Cascade," ASME Paper No. 79-GT-20.

Goldstein, R. J., and Chen, H. P., 1985, "Film Cooling on a Gas Turbine Blade Near the End Wall," ASME *Journal of Engineering for Gas Turbines and Power*, Vol. 107, p. 117.

Goldstein, R. J., Chyu, M. K., and Hain, R. C., 1985, "Measurement of Local Mass Transfer on a Surface in the Region of the Base of a Protruding Cylinder With a Computer-Controlled Data Acquisition System," *International Journal of Heat and Mass Transfer*, Vol. 28, p. 977.

Goldstein, R. J., and Karni, J., 1984, "The Effect of a Wall Boundary Layer on Local Mass Transfer From a Cylinder in Crossflow," ASME JOURNAL OF HEAT TRANSFER, Vol. 106, p. 260.

Goldstein, R. J., and Taylor, J. R., 1982, "Mass Transfer in the Neighborhood of Jets Entering a Crossflow," ASME JOURNAL OF HEAT TRANSFER, Vol. 104, p. 715.

Graziani, R. A., Blair, M. F., Taylor, J. R., and Mayle, R. E., 1980, "An Experimental Study of Endwall and Airfoil Surface Heat Transfer in a Large Scale Turbine Blade Cascade," ASME *Journal of Engineering for Power*, Vol. 102, p. 257.

Hah, C. A., 1984, "A Navier-Stokes Analysis of Three-Dimensional Turbulent Flows Inside Turbine Blade Rows at Design and Off-Design Conditions," ASME *Journal of Engineering for Gas Turbines and Power*, Vol. 106, No. 2, p. 421.

Hennecke, D. K., 1982, "Turbine Blade Cooling in Aeroengines," von Karman Institute for Fluid Dynamics, Lecture Series 1982-02, and personal communication.

Ito, S., 1976, "Film Cooling and Aerodynamic Loss in a Gas Turbine Cascade," Ph.D. Thesis, University of Minnesota, Minneapolis, MN, p. 127.

Kan, S., Miwa, K., Morishita, T., Munakata, Y., and Normura, M., 1971, "Heat Transfer of a Turbine Blade," *Tokyo Joint Int. Gas Turbine Conf.*, Paper No. JSME-30.

Langston, L. S., 1980, "Crossflows in a Turbine Cascade Passage," ASME *Journal of Engineering for Power*, Vol. 102, p. 866.

Marchal, Ph., and Sieverding, C. H., 1977, "Secondary Flows Within Turbomachinery Bladings," AGARD Conf. Proc., No. 214.

Metzger, D. E., and Mayle, R. E., 1983, "Gas Turbine Engines," *Mechanical Engineering*, p. 44.

Moffat, R. J., 1982, "Contribution to the Theory of Single Sample Uncertainty Analysis," ASME *Journal of Fluids Engineering*, Vol. 104, pp. 250.

Schlichting, H., 1979, *Boundary Layer Theory*, 7th ed., McGraw-Hill, New York, pp. 641, 710.

Sieverding, C. H., 1985, "Recent Progress in the Understanding of Basic Aspects of Secondary Flows in Turbine Blade Passages," ASME *Journal of Engineering for Gas Turbines and Power*, Vol. 107, pp. 248–257.

Sonoda, T., 1985, "Experimental Investigation on Spatial Development of Streamwise Vortices in a Turbine Inlet Guide Vane Cascade," ASME Paper No. 85-GT-20.

Sparrow, E. M., Stahl, T. J., and Traub, P., 1984, "Heat Transfer Adjacent to the Attached End of a Cylinder in Crossflow," *Int. Journal Heat Mass Transfer*, Vol. 27, No. 2, pp. 273–242.

York, R.E., Hylton, L. D., and Mihelc, M. S., 1984, "An Experimental Investigation of Endwall Heat Transfer and Aerodynamics in a Linear Vane Cascade," ASME *Journal of Engineering for Gas Turbines and Power*, Vol. 106, p. 159.